Fission product yield measurements using monoenergetic photon beams

Krishichayan, Megha Bhike, C. R. Howell, A. P. Tonchev, and W. Tornow

Fission Product Yield Measurements using Monoenergetic Photon Beams

Krishichayan,[1,][*] Megha Bhike,[1] C. R. Howell,[1] A.P. Tonchev,[2] and W. Tornow[1]

[1] *Department of Physics, Duke University, Durham, North Carolina 27708, USA*
and
Triangle Universities Nuclear Laboratory, Durham, North Carolina 27708, USA
[2] *Nuclear and Chemical Sciences Division, Lawrence Livermore National Laboratory, Livermore, California 94550, USA*
(Dated: June 5, 2019)

Background   High-accuracy and self-consistent fission product yield (FPY) data are needed to advance microscopic/macroscopic descriptions of the nuclear fission process, to improve the predictive power of phenomenological models, and for applications in nuclear energy, nuclear forensics, and homeland security.

Purpose   In a collaboration between the Triangle Universities Nuclear Laboratory (TUNL), Los Alamos National Laboratory (LANL), and Lawrence Livermore National Laboratory (LLNL), the dependence of a number of cumulative FPYs on the incoming neutron energy has been measured and unexpected energy dependencies of certain fission products have been reported [1]. To investigate whether this observation is unique to neutron-induced fission, a program has been initiated to measure FPYs in photon-induced fission.

Method   The photon-induced FPYs were measured by a combination of fission counting using a specially designed dual-fission chamber and γ-ray counting. The measurements were carried out with a monoenergetic photon beam at the HIγS facility. Gamma-ray counting of the activated targets were performed with well-shielded HPGe detectors over a period of two months post irradiation to properly identify the decay history of fission products.

Results   We report on our photofission product yield measurements on ^{235}U, ^{238}U, and ^{239}Pu using a monoenergetic photon beam of $E_\gamma = 13$ MeV. More than 40 fission products were uniquely identified, and their yield values were computed. The use of the fission chamber with post activation measurements has provided absolute fission product yield data with minimal uncertainties.

Conclusion   The photon-induced cumulative fission product yields of ^{235}U, ^{238}U, and ^{239}Pu are compared with previous photon- and neutron-induced fission measurements. In the near future data will be obtained at lower and higher photon energies.

PACS numbers:

I.   INTRODUCTION

Nuclear fission is a highly complicated nuclear reaction phenomenon. An understanding of observables resulting from nuclear fission requires information on both static nuclear properties and large-scale nuclear dynamics, as well as the understanding of nuclear structure configurations in extreme conditions, and the respective strengths of collective and single-particle degrees of freedom [2]. The process of nuclear fission starts with the formation of a compound nucleus which could be produced through a variety of excitation mechanisms, each with its own peculiarities. Particle bombardment is one such means and tends to produce an initial nucleus with high angular momentum and excitation energy. For this reason, particle-induced fission is useful for studying a regime of fission that is either minimally sensitive to the shell structure or involves high angular momentum. The use of real photons, on the other hand, preferentially pro-

duces low-spin configurations at all energies. Because the photon carries spin 1, only a restricted number of compound nucleus states are available from which fission can take place and this in turn reduces the complexity of the fission mechanism. Extraction of information from reactions with real photons is, therefore, less complicated and can be potentially better understood. That is even more true when the incident photons are monoenergetic, reducing the excitation energy of the compound nucleus to a desired narrow energy region. Fission induced by photons, photofission, is therefore, a useful method for investigating the low-energy regime, which is the most important one for practical applications. Precise photon-induced fission measurements are important in a variety of research and development areas, *e.g.*, basic nuclear physics, remote detection of nuclear materials, nuclear forensic, physics and technology in fission reactors, characterization and transmutation of nuclear waste [3–8].

The key to understanding the fission process and therefore the underlying nuclear dynamics lies in relatively few observables: fission cross section, total kinetic energy release, prompt neutron and γ-ray multiplicity, fission product yields, and neutron multiplicities. The measurements of the fission product yield is one of the main

---

*Electronic address: krishi@tunl.duke.edu\&krishichayan@ gmail.com

quantities used to test models of the reaction dynamics and associated nuclear structure.

The main need for fission product yield data comes from stockpile stewardship and nuclear forensic applications, as well as from any type of modeling associated with situations where actinides are being, or have been fissioned. In the nuclear reactor industry the primary use of these data involves fuel cycle calculations, including those on decay heat, shielding, dosimetry, burn-up, waste disposal, and safety.

Fission product yields have historically been one of the most studied observables of fission. A collaboration between TUNL, LANL, and LLNL has recently provided data on the energy dependence of high-yield FPYs from monoenergetic neutron-induced fission of ^{235}U, ^{238}U, and ^{239}Pu between thermal and 14.8 MeV [1, 9, 10]. According to this work, the cumulative FPYs obtained for ^{239}Pu show a peculiar energy dependence for certain high-yield fission products like ^{99}Mo, ^{140}Ba, and ^{147}Nd. The energy dependency of the FPYs for these nuclei has a positive slope at incident neutron energies below about 5 MeV and then becomes negative at higher neutron energies. This is in contrast to the same FPYs from ^{235}U$(n,$f$)$.

There is a scarcity of photofission data obtained with monoenergetic photons. This situation is mainly because of the lack of intense sources of monoenergetic photon beams. Most of the photofission cross section and FPY measurements have been carried out using bremsstrahlung beams. Measurements of an excitation function with a bremsstrahlung beam is technically very challenging and has substantial uncertainties caused by subtraction of large numbers. A standard technique for determining excitation function with bremsstrahlung beam is to increase the end-point energy of the beam in small increments over the energy range of interest [11]. This method requires high stability in the accelerator parameters, enormous counting statistics, and high-precision knowledge of the flux and the shape of the bremsstrahlung energy spectrum, especially near the end-point energy. Table I lists the previous FPY measurements of ^{235,238}U$(\gamma,$f$)$ and ^{239}Pu$(\gamma,$f$)$ at energies of interest in the present work.

A program has been initiated at TUNL to carry out systematic comparisons of the FPYs from neutron and photon induced fission on actinide nuclei, starting with ^{235,238}U and ^{239}Pu. For both (n,f) and (γ, f) reactions, the incident beam is monoenergetic, both measurements cover approximately the same range of excitation energies, and the same isotopes will be tracked in the FPY measurements. This study is intended to provide insight about the dependence of the FPY on the mechanism for inducing fission in the entrance channel. In particular, differences in the FPY for neutron and gamma induced fission would indicate a connection between the FPY and the angular momentum of the excited compound nucleus that fissions. Included in this program are direct tests of the Bohr Hypothesis [34] on nuclear fission, i.e., the exit channel products in fission have direct connection

TABLE I: Previous FPY measurements of the ^{235,238}U$(\gamma,$f$)$ and ^{239}Pu$(\gamma,$f$)$ reactions at energies of interest in the present work.

First Author	Year	E$_\gamma$ range (MeV)	Beam
^{235}U			
Kondrat'ko [12]	1966	10.0 - 25.0	bremsstrahlung
Petrzhak [13]	1969	12.1 - 25.0	bremsstrahlung
Aumann [14]	1970	13.8, 16.8, 17.1	bremsstrahlung
Kondrat'ko [15]	1973	14.0	bremsstrahlung
Petrzhak [16]	1976	20.0	bremsstrahlung
Thierens [17]	1976	25.0	bremsstrahlung
Jacobs [18]	1980	12.0 - 70.0	bremsstrahlung
Carrel [19]	2011	16.3, 19.3	bremsstrahlung
^{238}U			
Petrzhak [20]	1963	14.0	bremsstrahlung
Aumann [14]	1970	13.8, 16.8, 17.1	bremsstrahlung
Petrzhak [21]	1971	15.0	bremsstrahlung
Alm [22]	1973	4.65 - 6.6	bremsstrahlung
Thierens [17]	1976	25.0	bremsstrahlung
Jacobs [23]	1979	12.0 - 70.0	bremsstrahlung
Kahane [24]	1985	7.8	(n,γ)
Gangrsky [25]	2003	25.0	bremsstrahlung
Naik [26]	2011	10.0	bremsstrahlung
Carrel [19]	2011	16.3, 19.3	bremsstrahlung
Naik [27]	2013	11.5 - 17.3	bremsstrahlung
Naik [28]	2014	8.0	bremsstrahlung
Belyshev [29]	2015	19.5 - 67.7	bremsstrahlung
Wen [30]	2016	22.0	bremsstrahlung
^{239}Pu			
Kondrat'ko [31]	1976	10.0 - 24.0	bremsstrahlung
Kondrat'ko [32]	1981	28.0	bremsstrahlung
Wen [30]	2016	22.0	bremsstrahlung
Bhike [33]	2017	11.0	monoenergetic photon

to the details of the entrance channel. For example, we are starting to perform ^{239}Pu(n,f) and ^{240}Pu$(\gamma,$f$)$ cross-section and FPY measurements at the same excitation energy. Such measurements will enable direct comparisons of the two processes.

Our exploratory study [33] of photofission of ^{239}Pu at E_γ = 11 MeV has provided data for eight fission products. The associated uncertainties were around 10-15%. The photon beam flux was determined from the ^{197}Au$(\gamma,$n$)^{196}$Au reaction, which contributed significantly to the uncertainty of these FPY values.

In the present work, we report on our high-accuracy measurements of the fission product yields from photofission of ^{235}U, ^{238}U, and ^{239}Pu at a photon energy of E_γ = 13 MeV. The measurements were carried out using monoenergetic photon beams provided by the High Intensity γ-ray Source (HIγS) facility at TUNL. The techniques employed do not require absolute determination of the gamma-ray beam flux, thus significantly reducing the systematic uncertainties in the FPY measurements relative to previous results. The data reported in this work represent the beginning of a project aimed at obtaining FPYs for important fission products as a function of incident photon energy. Preliminary results of this work have been published in Ref. [35].

The following sections describe and discuss the main features of the experimental methods, the data analysis and results, and the comparison of our photofission results with data from bremsstrahlung- and neutron-induced FPY measurements and conclude with a summary of our results and findings.

II. EXPERIMENTAL DETAILS

The HIγS, located on the campus of Duke University, generated circularly polarized and monoenergetic photon beams for the present experiment. Details on the HIγS facility can be found in Ref. [36] and are briefly summarized here. The HIγS facility produces a quasi-monoenergetic Compton backscattering photon beam tunable over a wide energy range with either linear or circular polarization. A high-flux photon beam is created by colliding relativistic electron beam bunches, circulating in a storage ring, with photon pulses inside the high-power optical cavity of a free-electron laser (FEL). The electron beam current was $\sim$ 100 mA. The electron beam energy was $\sim$ 623 MeV and the FEL photon wave length was 546.5 nm, resulting in a 13.0 MeV photon beam. This beam passed through an Al collimator of length 44.5 cm with a cylindrical hole of 1.27 cm diameter and positioned 55 meters downstream from the FEL photon-electron collision point in the storage ring. This collimator diameter results in an energy spread of $\sim$ 2% (FWHM) of the photon beam centroid energy. Aluminum was chosen as the collimator material to avoid neutrons produced via the (γ,n) reaction because of its high neutron separation energy of 13.6 MeV.

A schematic of the experimental setup in the upstream target room of the HIγS facility is shown in Fig. 1, where the photon beam from the FEL storage ring comes from the left side. A key part of the setup is the dual-fission chamber (DFC) and is described in the next section. The
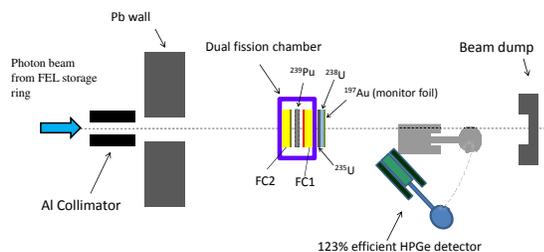

FIG. 1: (Color online) Schematic diagram (not to scale) of the experimental setup using a dual-fission chamber and a 123% efficient (relative) HPGe detector. Placement of three actinides and Au monitor foil are also shown.

DFC was placed at a distance of $\sim$ 58 m from the FEL collision point, which eliminates the need for a source-target angular-correlation correction, because the same collimated photon flux is seen by both chambers and the

actinide targets being irradiated.

III. DATA ANALYSIS

A. FPY Determination

In practice, the accurate determination of the photon beam flux (ϕ) can be very challenging, and can be the main source of systematic uncertainty in FPY measurements. The use of our DFC provided an alternative approach to determine the total number of fission events in the target without having to explicitly know the fission cross section or the photon flux, thus greatly reducing the systematic uncertainty in the measurements. The FPY refers to the fraction of a fission product produced per fission, and is usually stated as percentage per fission, so that the total yield sums to 200%, and is related to the total fission cross section (σ_f) and the cross section to produce a certain fission product (σ_{FP}) through the (γ,f) reaction as given below:

$$FPY = \frac{\sigma_{FP}}{\sigma_f}. \quad (1)$$

The DFC provides the quantity $\sigma_f \Phi$, which is equal to the fission rate, F_T, that occurred in the target. This, along with Eq. 1, can be substituted into the activation equation [37–39], which leads to the following expression for the FPY,

$$FPY = \frac{\lambda N_\gamma}{F_T N_a (1 - e^{-\lambda t_i}) e^{-\lambda t_d}}. \quad (2)$$

This expression can be re-written for each fission fragment as follows:

$$FPY = \frac{\lambda N_\gamma}{F_T N_a I_\gamma \epsilon} \frac{1}{1 - e^{-\lambda t_i}} \frac{1}{e^{-\lambda t_d}} \frac{1}{1 - e^{-\lambda t_m}} C_f, \quad (3)$$

where,
λ = decay constant
N = number of γ-rays from photo-peak
N_a = number of target nuclei
I_γ = intensity of the γ-ray transition
ϵ = full-energy peak efficiency of HPGe detector
F_T = fission rate in target determined from DFC
t_i = time of irradiation or activation
t_d = decay time from the end of activation
t_m = measurement time
C_f = correction factors: beam fluctuation, attenuation, isotope correction

A key component in obtaining accurate FPY data is the precise quantitative determination of the number of fissions which occur during the measurements. To accomplish this, a specially fabricated dual-fission ionization chamber (DFC) was used, as shown in the experimental setup (Fig.1). Such fission chambers have extensively

been used in our neutron-induced FPY measurements. Details of a DFC can be found in [1, 40] and they are briefly summarized here. The dual-fission chamber was adopted from the design developed by Gilliam *et al.* at NIST [41]. However, several design changes were made to facilitate the insertion and removal of the activation target contained between the two individual fission chambers (FCs). The gas connections to the individual FCs are made of stainless steel tubing. The signals from each of the FCs are sent to the manifold via a UT-085 semi-rigid coaxial cable that runs inside the gas line. P-10 (90% argon and 10% methane) was used as the DFC fill gas. Signals from the FCs are input to ORTEC 142-PC preamplifiers. The preamplified signals are then amplified by a Canberra 2026 spectroscopic amplifier and then fed to a Canberra Multiport II multichannel analyzer, supported by the GENIE 2000 software [42].

For the present photon-induced measurement, two thin reference foils (^{235}U in chamber 1 and ^{239}Pu in chamber 2) were used. The ^{239}Pu thick activation target was placed at the center of the fission chamber and the two other actinide samples were placed outside at the downstream end of the fission chamber (see Fig. 1). For ^{238}U, the photon flux was calculated using the total number of fission events recorded in the ^{235}U fission chamber and the corresponding ^{235}U(γ, f) cross section at 13.0 MeV (357.8 mb from Ref. [43]).

Detailed information about the reference foils and activation targets used in the present work is given in Table II. The mass of the reference foils was determined by alpha spectroscopy using well-calibrated ionization chambers at LANL. The uncertainty in the mass of the foils is ±1%, which is a conservative estimate of the systematic error in the measurement method. Typical pulse-height fission spectra produced by the DFC during the photon irradiation are shown in Fig. 2. They are integrated to give the total number of fissions recorded in the individual chambers.

TABLE II: Information on the reference foils and activation targets used in the present experiment. The diameter of each reference foil and activation target is 1.27 cm.

Reference foil	Chamber #	Mass (μg)	Isotopic abundance(%)
^{235}U	FC1	160.36(160)	99.835(2)
^{239}Pu	FC2	8.52 (3)	99.954(2)

Activation target	Mass (mg)	Isotopic abundance(%)
^{235}U	223.02(2)	93.27(3)
^{238}U	236.6(6)	99.70(8)
^{239}Pu	233.0(2)	98.41(40)

A 123% efficient (relative to a standard 7.62 cm x 7.62 cm NaI detector) coaxial HPGe detector was placed downstream of the fission chamber position to measure the beam-energy distribution. During beam-energy measurements, the photon beam was attenuated by a series of copper attenuators mounted upstream, approximately
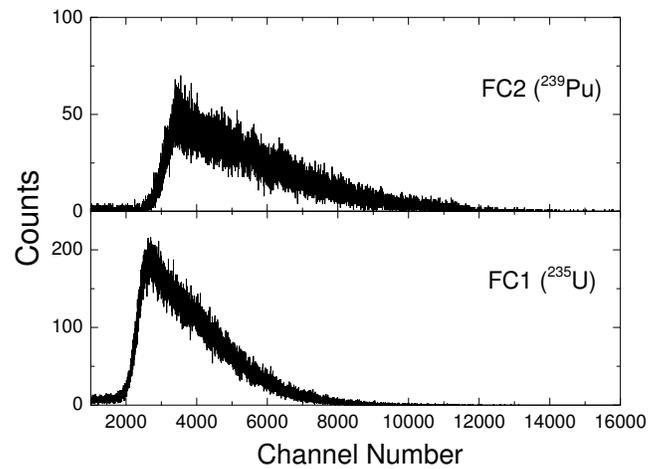

FIG. 2: Fission chamber pulse-height spectra for the downstream (FC1) and upstream (FC2) chambers are shown for a 13.0 MeV incident photon beam. These chambers were loaded with ^{235}U and ^{239}Pu, respectively.
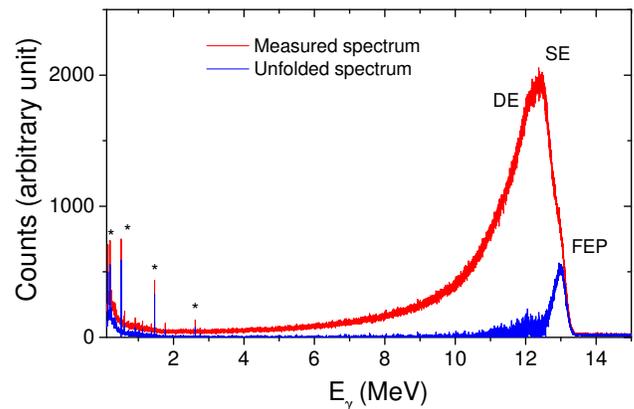

FIG. 3: (Color online) γ-ray energy spectrum (in red) measured with a 123% HPGe detector positioned at 0° relative to the incident photon beam axis. The full-energy peak (FEP) at 13 MeV, single escape (SE), and double escape (DE) are labeled. In the low-energy part of the spectrum, room background lines (indicated by the asterisk) are clearly seen. Taking the HPGe detector response in to account, the unfolded spectrum of the FEP (shown in blue) is obtained.

45 m from the location of the DFC. The energy variation in the attenuation coefficient is negligible over the narrow energy width of the beam, resulting in a negligible distortion of the beam energy profile.

The spectra from these measurements were unfolded to correct for the detector response in order to determine the beam-energy profile. A typical energy distribution of the incident beam is shown in Fig. 3. The FWHM resolution of the beam at 13 MeV is $\sim$ 250 keV ($\sim$ 2.0%). The uncertainty in its centroid energy is less than ±10 keV. After the beam-energy measurement, the HPGe detector and attenuators were moved to an off-axis position during the actual irradiation measurements.

A ^{197}Au monitor foil was also irradiated along with the three actinides to determine the photon flux via ^{197}Au(γ,n)^{198}Au reaction to cross check the flux obtained from the ^{235}U and ^{239}Pu monitor foils in the fission chamber. A good agreement was found within the associated uncertainties after attenuation corrections were applied. Although not needed for determining the FPYs the incident photon flux was found to be $\sim 1 \times 10^8$ $\gamma/(\text{cm}^2\text{s})$.

B. Gamma-ray counting

After 62 hours of continuous irradiation with $\sim 10^8$ $\gamma/(\text{cm}^2\text{s})$, the target samples (^{235}U, ^{238}U, and ^{239}Pu) and ^{197}Au monitor foil were γ-ray counted in TUNL's low-background counting facility using high-efficient (55 - 60 % relative efficiency to 7.62 cm x 7.62 cm NaI detector) HPGe detectors over a period of two months after activation using a number of different counting cycles. These detectors are elaborately lead-shielded against room- and cosmic-ray background radiations. Each irradiated sample was placed in a plastic (acrylic) container and positioned at a distance of 5 cm from the front face of the detector for the counting measurements. A Canberra Multiport II multi-channel analyzer was used for the data-acquisition system and spectra were accumulated using the GENIE-2000 software [42] with active pile-up rejection. Because the photo-peak count rate in the γ-ray spectrum is used to determine the activity of the sample, the efficiency of each detector was determined accurately using a mixed nuclide γ-ray source obtained from Eckert & Ziegler [44] under identical conditions to those used for counting the actinide targets and monitor foil. Mixed γ-ray sources are useful since a number of energies (ranging from 59.54 to 1836.06 keV) can be measured simultaneously rather than repeating efficiency measurements with separate sources. Because the majority of the nuclides in the mixed source are single γ-ray emitters and therefore, are not in coincidence with any other transitions, coincidence summing effects are practically eliminated. Figure 4 shows the efficiency curve for one of the 55% efficient HPGe detectors. The program "effit" from the RADWARE package [46] was used to fit the individual efficiency data values.

Representative γ-ray spectra for the three actinide samples are shown in Fig. 5. As seen clearly, the ^{239}Pu spectrum is more complicated than that for the ^{235}U and ^{238}U isotopes, where a less background is seen in the low energy regime. Specific cases of decay spectra are shown in Figs. 6, 7, and 8, where γ rays belonging to ^{87}Kr, ^{142}La, ^{91}Sr, ^{135}I, ^{97}Zr, and ^{91}Sr fission products are shown for two different counting conditions. These decay spectra were used to uniquely identify the products and to ensure that no interfering transitions were present. Based on these data, decay activity curves for each fission product were constructed, and the half-lives of the fission products were determined from the cycle measurements and compared to literature values. Typical decay curves for
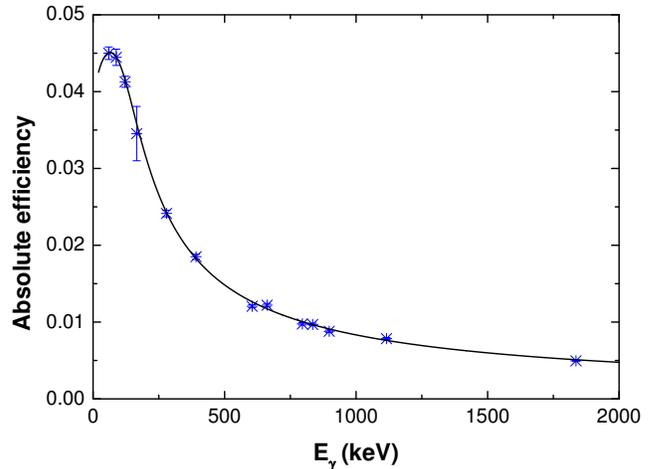

FIG. 4: (Color online) Measured absolute efficiency for one of the HPGe detectors using a mixed nuclide γ-ray source. The solid curve is the fit to the data values (see text for details). The large error associated with the 165.8 keV γ ray is due to the uncertainty in our knowledge of the intensity of this line ($I_\gamma \sim 10\%$) [45].

the fission products from three actinides are shown in Fig. 9. The associated half-life times for the fission products are in good agreement with the literature values [45] except for some of the weak products where the half-life deviation is up to 10%. Several products, such as ^{135}Xe or ^{140}La, are produced directly from fission and as daughter nuclei from other fission product parents with similar or longer half-lives. In such cases, fitting and deconvoluting the decay curves is necessary to determine the number of nuclei produced at t = 0 (end of activation). Extensive background measurements were performed prior to irradiation, in identical geometrical conditions as the counting of the activated targets to check on interferences in the region of interest due to the background from target radioactivity prior to irradiation.

The relevant nuclear spectroscopic data for the fission products measured in the present work were taken from Ref. [45] and are given in Table III.

C. Uncertainties

A major part of the systematic uncertainty in this measurement comes from errors associated with the detector efficiency and photo-peak area analysis. A summary of the sources of uncertainties and their estimated magnitudes is tabulated in Table IV. The statistical uncertainties of the photo-peak areas were typically in the order of 1-2%, and only for a limited number of γ-ray transitions the uncertainties were larger, resulting in the range of values given in the table. The error bars on our data in the plots represent the total experimental uncertainties,
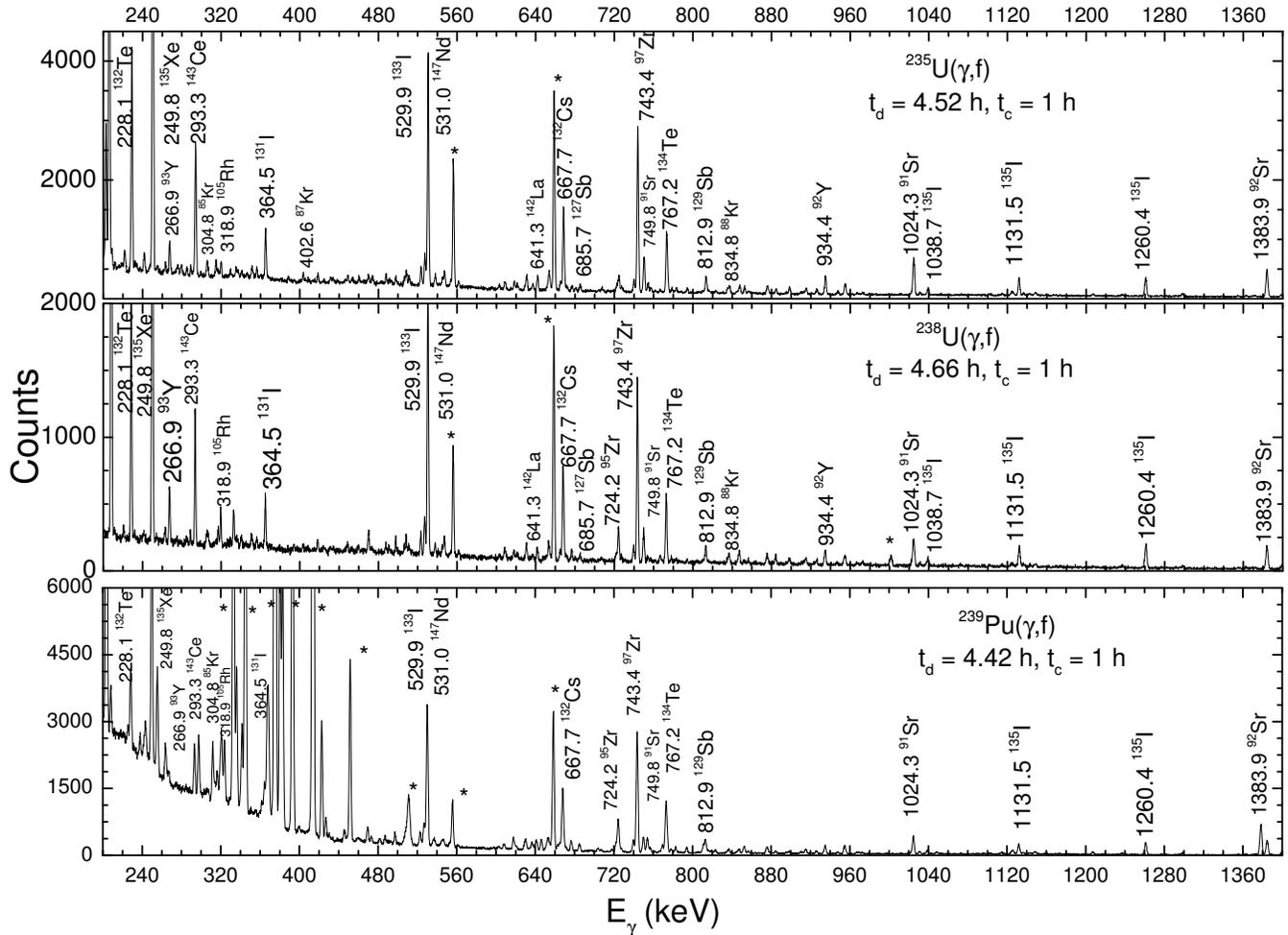
FIG. 5: Typical γ-ray spectra of fission products from ^{235}U(γ,f), ^{238}U(γ,f), and ^{239}Pu(γ,f). Counting conditions (decay and measurement times) are also given. The unidentified and/or background γ-transitions are marked by the asterisks.

which were computed by adding statistical and systematic uncertainties in quadrature.

IV. RESULTS AND DISCUSSION

More than 40 fission products were observed and absolute cumulative FPYs for ^{235}U, ^{238}U, and ^{239}Pu were determined, covering a large range of nuclides in terms of half-lives ranging from ~ 20 minutes to ~ 32 days. The analysis procedures closely followed those described in Ref. [1].

The results for the cumulative FPYs of the fission products studied in the present work are tabulated in Table V. They range from as low as 0.10% (^{136}Cs from photofission of ^{239}Pu) to as high as 9.53% (^{93}Y from photofission of ^{238}U). The FPY distributions for photofission of ^{235}U, ^{238}U, and ^{239}Pu are shown in Fig. 10. For all three cases, the light product mass-

distribution is smoother than that for the heavy product mass-distribution. For ^{239}Pu the light fragment mass-distribution is shifted to heavier masses compared to ^{235}U and ^{238}U, while for the heavy products the opposite trend is observed. The difference between ^{235}U and ^{238}U FPY distributions is less pronounced, except for the light-yield values of ^{92,93}Y found for ^{238}U, although their uncertainties are fairly large.

A. ^{235}U

There exist quite a number of bremsstrahlung-beam-induced FPY measurements for the ^{235}U(γ,f) reaction in the energy range of $E_\gamma \sim 10.0$ - 20.0 MeV. Most of these experiments were carried out during the 1970s by Kondrat'ko *et al.* [12, 15], Petrzhak *et al.* [13, 16], Aumann *et al.* [14], and Thierens *et al.* [17]. In 1980 Jacobs *et al.* [18] measured and compared the mass chain yield
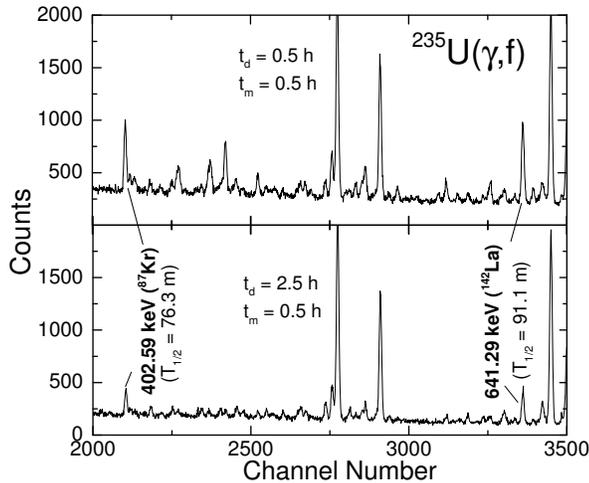
FIG. 6: Spectra showing γ rays from the decay of the fission products [87]Kr (half-life = 76.3 m) and [142]La (half-life = 91.1 m) after photofission of [235]U. The characteristics γ-ray lines are indicated. The counting conditions (decay and measurement times) are also given.
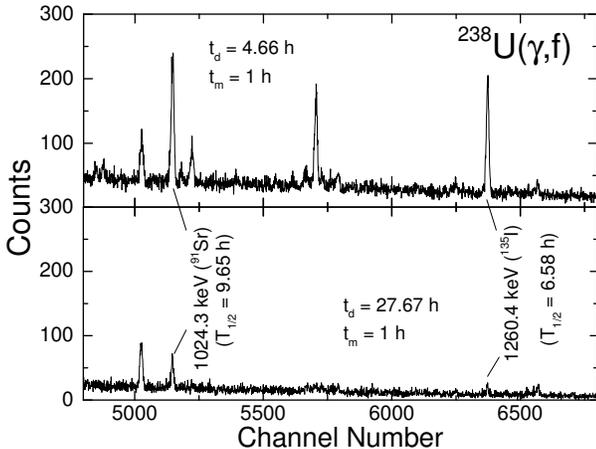

FIG. 8: Spectra showing γ rays from the decay of the fission products [97]Zr (half-life = 16.75 h) and [91]Sr (half-life = 9.65 h) after photofission of [239]Pu. The characteristics γ-ray lines are indicated. The counting conditions (decay and measurement times) are also given.

FIG. 7: Spectra showing γ rays from the decay of the fission products [91]Sr (half-life = 9.65 h) and [135]I (half-life = 6.58 h) after photofission of [238]U. The characteristics γ-ray lines are indicated. The counting conditions (decay and measurement times) are also given.

FIG. 9: Decay curves of [142]La, [92]Sr, and [91]Sr fission products (from [235]U(γ,f), [238]U(γ,f), and [239]Pu(γ,f), respectively). The solid lines are the fits to the measured data. The γ-ray transitions used for these nuclei are listed in Table III. Note the logarithmic (base e) scales on the activity axis.

of fission products for the photofission of [235]U with 12.0 to 70.0 MeV bremsstrahlung beams. More recently, in 2011, Carrel *et al.* [19] presented new experimental results on the cumulative yields from photofission of [235]U induced by 16.3 and 19.3 MeV end-point bremsstrahlung beams. An approach of simultaneous detection of delayed neutrons and delayed γ rays was applied in their experimental technique.

Our FPY data obtained with a monoenergetic photon beam at 13.0 MeV are compared in Fig. 11 to FPY data measured with bremsstrahlung beams of end-point energies of 12 [18], 16.3 [19], and 25 MeV [17]. Jacobs
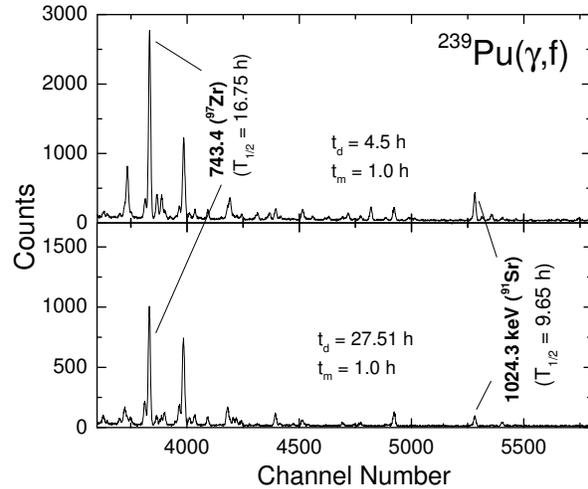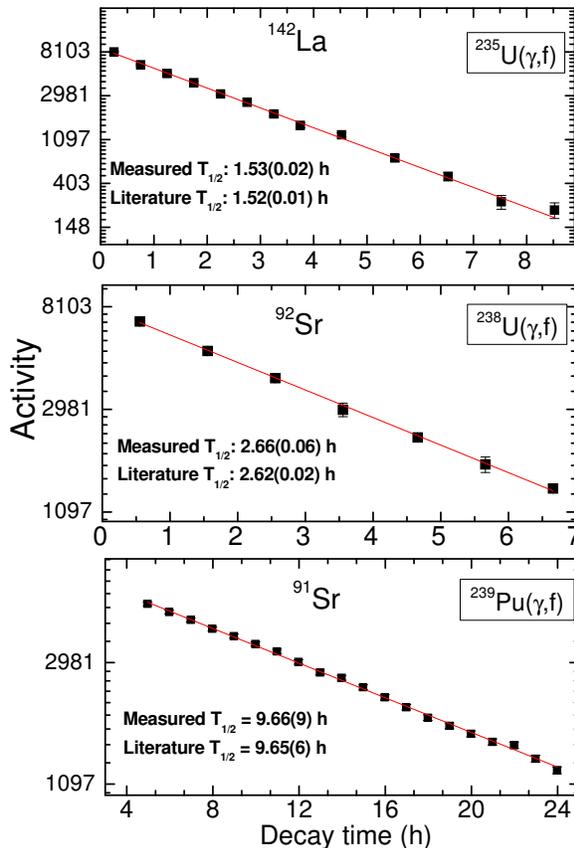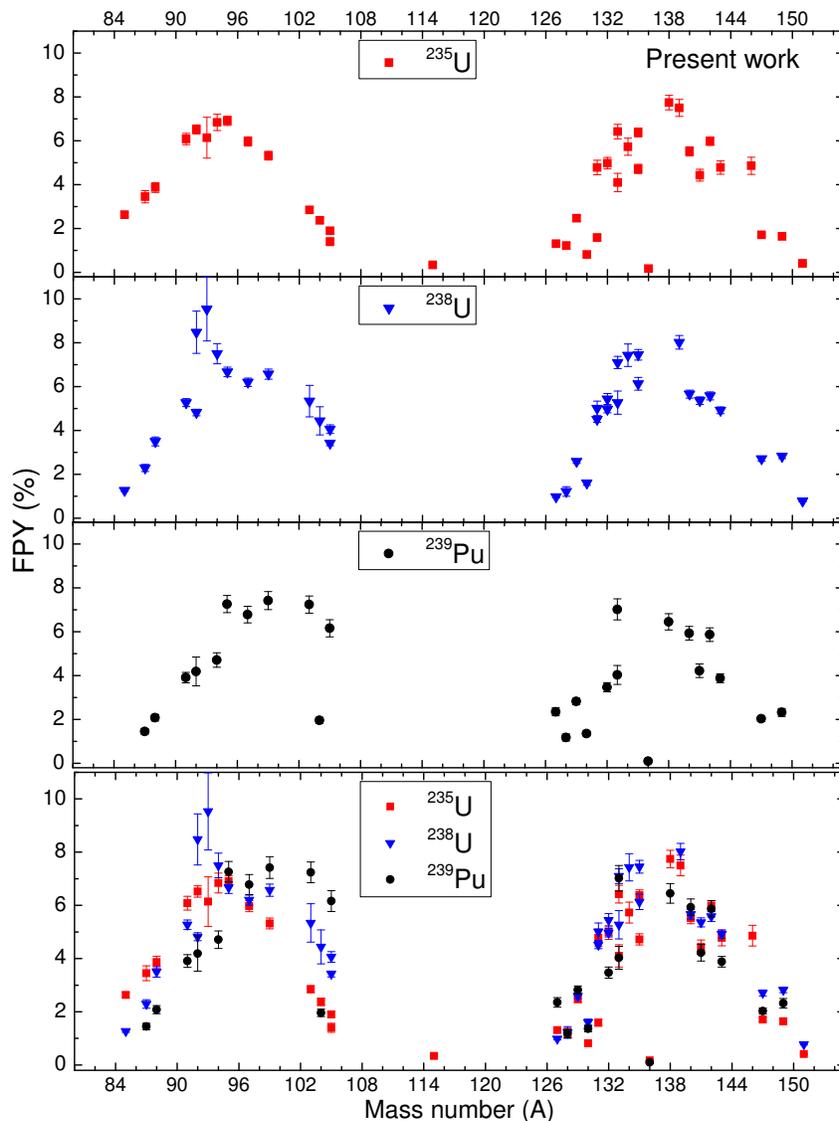
FIG. 10: (Color Online) Plot of the FPY distributions measured in the present photofission of ^{235}U, ^{238}U, and ^{239}Pu at $E_\gamma =$ 13 MeV. The error bars on our data points represent the total experimental uncertainties. Lower panel shows the comparison of the FPY distributions.

et al. [18] and Thierens *et al.* [17] measured the total mass-chain yield of fission products. For the lighter fission products the agreement between all data sets is quite remarkable, while for the heavier products there is considerable scatter in the data.

The relative difference ($= 100\% \times$ (FPY$_{brem}$ - FPY$_{present}$)/FPY$_{present}$) between the bremsstrahlung data sets and present data is shown in Fig. 12. This presentation is consistent with the findings above and also suggests that the bremsstrahlung data obtained by Jacobs *et al.* [18] with end-point energy of 12 MeV is in slightly better agreement with our data than with the two other data sets of higher end-point energies. However, no firm conclusion can be drawn about a definitive energy dependence of the FPYs in the energy range studied in this work.

B. ^{238}U

There have been a handful of bremsstrahlung-beam-induced photofission studies on ^{238}U that measure yields of the fission products in the energy range of our present work. Similar to the ^{235}U(γ,f) work, most of the early measurements on ^{238}U were carried out in the 1970s by the same groups, e.g., Petrzhak *et al.* [20, 21], Aumann *et al.* [14], Thierens *et al.* [17], Jacobs *et al.* [23]. Kahane *et al.* [24] measured fission yields from the photofission of ^{238}U with neutron capture γ rays at an effective excitation energy of 7.8 MeV. In recent years, Naik and his group [19, 26–28] have measured the FPY values of several products from photofission of ^{238}U induced by bremsstrahlung beams with end-point energies from 8.0 to 20 MeV. Most of their measurements were

TABLE III: Nuclear data for identified fission products taken from chart of nuclides provided in the webpage of Ref. [45].

Fission Products	E_γ (keV)	$T_{1/2}$	I_γ (%)
^{84}Br	881.6	31.76(8) m	42.0
^{85}Kr^m	304.87	4.48(1) h	14.0(3)
^{87}Kr	402.6	76.3(5) m	50.0(30)
^{88}Kr	196.3	2.83(2) h	26.0(12)
^{91}Sr	1024.3	9.65(6) h	33.5(5)
^{92}Sr	1383.9	2.61(1) h	90.0(60)
^{92}Y	934.4	3.54(1) h	13.9(15)
^{93}Y	266.9	10.18(8) h	7.4(11)
^{94}Y	918.7	18.7(1) m	56.0
^{95}Zr	724.2	64.03(1) d	44.3(2)
^{97}Zr	743.4	16.75(1) h	93.1(10)
^{99}Mo	739.5	65.97(2) h	12.3(2)
^{104}Tc	358.0	18.3(3) m	89.0(9)
^{103}Ru	497.1	39.24(1) d	91.0(12)
^{105}Ru	724.3	4.44(2) h	47.3(10)
^{105}Rh	318.9	35.36(6) h	19.1(2)
^{115}Cd^g	336.2	53.46(5) h	45.9
^{127}Sb	685.7	3.85(5) d	36.8(4)
^{129}Sb	812.97	4.37(3) h	48.2(8)
^{130}Sb	793.4	39.5(8) m	100.0(50)
^{131}Sb	943.4	23.03(4) m	47.1
^{128}Sn	482.3	59.07(14) m	59.0(70)
^{132}Te	228.16	3.20(1) d	88.0(30)
^{133}Te	912.6	55.4(4) m	44.0(4)
^{134}Te	767.2	41.8(8) m	29.5(14)
^{131}I	364.5	8.02(1) d	81.5(8)
^{133}I	529.9	20.83(8) h	87.0(23)
^{135}I	1260.4	6.58(3) h	28.7(9)
^{135}Xe	249.8	9.14(2) h	90.0(10)
^{132}Cs	667.7	6.48(1) d	97.6(9)
^{136}Cs	1048.1	13.16(3) d	80.0(30)
^{138}Cs^g	1435.9	33.41(18) m	76.3(16)
^{139}Ba	165.86	1.38(1) h	23.8(4)
^{140}Ba	537.26	12.75(1) d	24.4(2)
^{141}Ba	190.3	18.27(7) m	45.5(20)
^{142}La	641.3	91.1(5) m	47.4(10)
^{141}Ce	145.4	32.51(1) d	48.4(4)
^{143}Ce	293.3	33.04(1) h	42.8(4)
^{146}Pr	453.8	24.09(10) m	46.0(30)
^{147}Nd	531.0	10.98(1) d	28.1(7)
^{149}Nd	211.3	1.728(1) h	25.9(14)
^{151}Pm	340.1	28.40(4) h	22.5(2)

TABLE IV: Sources of uncertainties and their estimated magnitudes. See text for details.

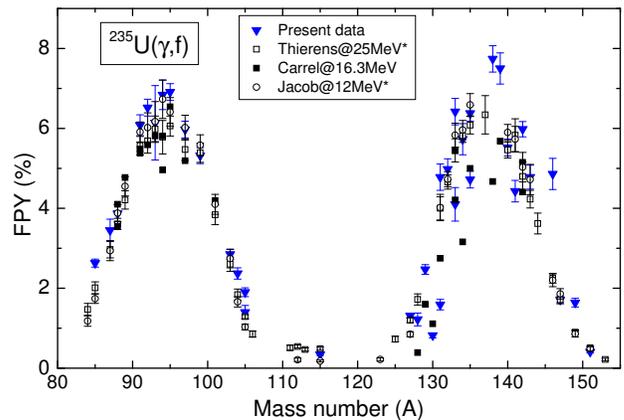| Source of Uncertainty	Magnitude (%)
Detector efficiency	2 -5
Photo-peak area	0.3 - 5
γ-ray intensity	0.1 - 5
Half-life	<0.6
γ-ray absorption	< 0.8
Target mass	0.01 - 0.1
Irradiation time	$\ll 1$
Decay time	$\ll 1$
Counting time	$\ll 1$
^{235}U(γ,f), ^{239}Pu(γ,f), and ^{197}Au(γ,n) cross sections	5

FIG. 11: (Color Online) FPY distributions of fission products in 12-[18], 16.3- [19], and 25-MeV [17] end-point bremsstrahlung-beam-induced fission of ^{235}U are compared with our present data obtained with monoenergetic photons at 13.0 MeV. The data marked with asterisks in the legends are the total mass-chain yield of fission products.

of about 11 fission products with half-lives in the range of those in our present work.

Figure 13 shows the present FPY data in comparison to FPYs obtained with bremsstrahlung beams of end-point energies between 8.0 and 25.0 MeV [17, 19, 20, 26–30]. Clearly, the bremsstrahlung-beam data do not support our large FPY results for ^{92,93}Y. This is an interesting observation which requires further study with monoenergetic photon beams of lower and higher energy than used in the present work to investigate whether or not nuclear structure effects might be at play.

The relative difference presented in Fig. 14 between the bremsstrahlung-beam data with end-point energies between 8 and 25 MeV and the present data at 13.0 MeV clearly shows that the majority of the FPYs measured with the bremsstrahlung beam is lower in magnitude than the present data. The FPY values obtained by Petrzhak et al. [21], Carrel et al. [19], and Wen et al. [30] with bremsstrahlung beams of end-point energies between 15.0 and 22.0 MeV are also consistently lower in

carried out using the electron linac facilities at Saclay, France and Mumbai, India. Recoil catcher and off-line γ-ray spectrometric techniques were used in these measurements. In 2015, Belyshev et al. [29] used the photon activation method to obtain the photofission total mass-chain distribution of ^{238}U after irradiation with bremsstrahlung beams of end-point energies of 19.5 - 67.7 MeV. In 2016, Wen and Yang [30] reported a technique to measure short-lived and relatively long-lived delayed γ rays from photofission of ^{238}U using a 10.0 MeV end-point bremsstrahlung beam. They measured the yields

TABLE V: FPY (in %) determined in the present 13 MeV monoenergetic photon-induced fission of ^{235}U, ^{238}U, and ^{239}Pu along with their total uncertainties.

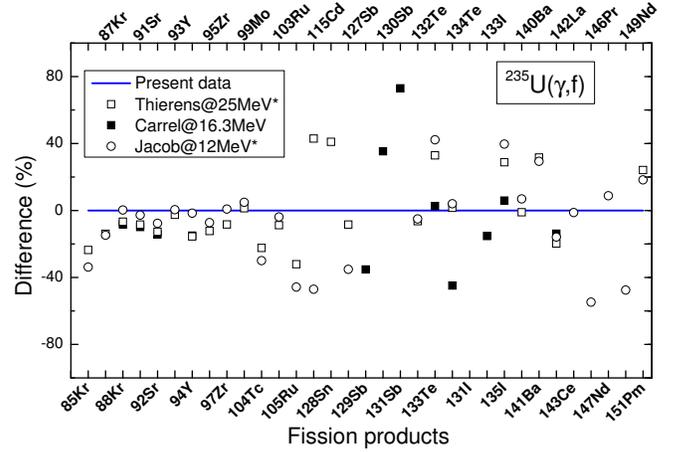| Product	FPY (%)		
	^{235}U	^{238}U	^{239}Pu
^{84}Br	1.77(13)	2.49(19)	-
^{85}Kr^m	2.63(10)	1.27(4)	-
^{87}Kr	3.45(28)	2.29(16)	1.45(12)
^{88}Kr	3.87(22)	2.92(17)	2.08(15)
^{91}Sr	6.08(26)	5.27(18)	3.91(24)
^{92}Sr	6.52(21)	4.82(15)	4.19(66)
^{92}Y	-	8.48(96)	-
^{93}Y	6.14(93)	9.53(145)	-
^{94}Y	6.84(37)	7.50(46)	4.71(33)
^{95}Zr	6.91(21)	6.67(22)	7.26(39)
^{97}Zr	5.97(21)	6.20(19)	6.78(38)
^{99}Mo	5.32(20)	6.57(22)	7.42(41)
^{104}Tc	2.37(14)	4.44(64)	1.96(14)
^{103}Ru	2.85(13)	5.34(72)	7.24(39)
^{105}Ru	1.90(11)	4.06(20)	6.16(39)
^{105}Rh	1.40(17)	3.42(11)	-
^{115}Cd^g	0.34(2)	-	-
^{128}Sn	1.22(16)	1.22(22)	1.18(16)
^{127}Sb	1.31(5)	0.98(4)	2.35(18)
^{129}Sb	2.47(12)	2.59(9)	2.82(15)
^{130}Sb	0.82(6)	1.61(11)	1.36(11)
^{131}Sb	1.59(13)	5.01(33)	-
^{132}Te	4.98(26)	5.44(25)	3.47(21)
^{133}Te	4.10(42)	5.27(53)	4.03(43)
^{134}Te	5.37(39)	7.43(51)	-
^{131}I	4.78(33)	4.51(14)	-
^{133}I	6.42(33)	7.10(28)	7.02(48)
^{135}I	4.72(21)	6.13(29)	-
^{135}Xe	6.38(20)	7.45(24)	-
^{132}Cs	-	4.97(16)	-
^{136}Cs ^{a}	0.17(1)	-	0.10(1)
^{138}Cs^g	7.74(33)	-	6.45(37)
^{139}Ba	7.50(39)	8.02(31)	-
^{140}Ba	5.52(21)	5.66(18)	5.93(31)
^{141}Ba	4.43(27)	-	4.22(31)
^{142}La	5.98(19)	5.58(18)	5.87(31)
^{141}Ce	-	5.36(17)	-
^{143}Ce	4.78(30)	4.92(15)	3.88(20)
^{146}Pr	4.86(39)	-	-
^{147}Nd	1.71(7)	2.71(11)	2.03(11)
^{149}Nd	1.64(11)	2.82(10)	2.32(18)
^{151}Pm	0.41(3)	0.78(3)	-

^{a}independent yield

FIG. 12: (Color Online) Differences (in %) between the previous FPY values of 33 fission products in 12.0 - 25.0 MeV end-point bremsstrahlung-beam-induced fission of ^{235}U [17–19] and our present data. The data marked with asterisks in the legends are the total mass-chain yield of fission products.

C. ^{239}Pu

There are only a few bremsstrahlung-beam-induced photofission studies on ^{239}Pu that measure yields of the fission products in the energy range of our work. In 1976 Kondrat'ko *et al.* [31] reported relative yields for a few photofission products of ^{239}Pu induced by 10.0 - 24.0 MeV end-point bremsstrahlung beams. Later in 1981, the same group [32] reported detailed FPY measurements on ^{239}Pu at a 28 MeV end-point bremsstrahlung beam. As in the case of ^{238}U, in 2016, Wen and Yang [30] reported FPY measurements for ^{239}Pu at a 10.0 end-point bremsstrahlung beam. They measured yields of about 13 fission products with half-lives in the range of our present work. In our exploratory study [33] we have measured yields of eight fission products from photofission of ^{239}Pu induced by monoenergetic photons at $E_\gamma =$ 11.0 MeV. In this exploratory work, a different approach was used to measure the photon beam flux which resulted in significantly higher uncertainties in the FPY values.

The present FPY distribution of the fission products obtained in photofission of ^{239}Pu are plotted in Fig. 15 in comparison to those measured with bremsstrahlung beams with end-point energies of 22 and 28 MeV [19, 30]. Compared to ^{235}U(γ,f) and ^{238}U(γ,f), the number of available FPY data for ^{239}Pu(γ,f) is considerably smaller. Also shown in this figure are previously reported FPY data obtained in our exploratory measurement with a monoenergetic photon beam of 11.0 MeV [33].

The relative difference between the bremsstrahlung FPY data of Wen *et al.* [30] and Kondrat'ko *et al.* [32] and our data is illustrated in Fig. 16. While the FPYs of Wen *et al.* [30] are in good agreement with our data, the data of Kondrat'ko *et al.* [32] are on the average approx-

magnitude than our FPY values. This finding is in stark contrast to the FPYs of ^{235}U, where the difference in our present values and those from bremsstrahlung beams are highly scattered (see Fig. 12).
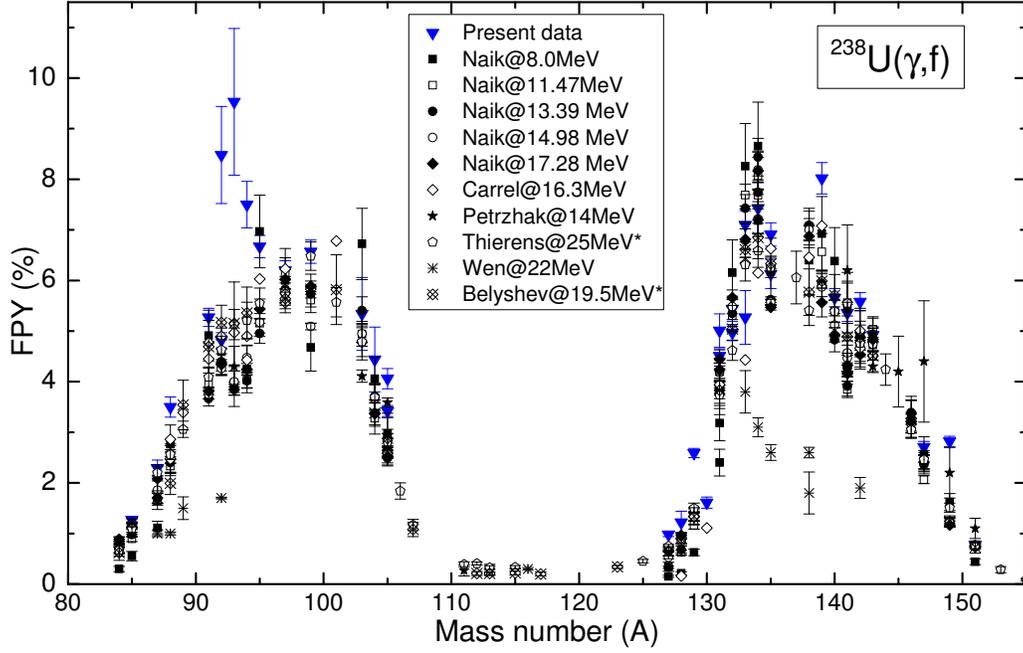
FIG. 13: (Color Online) Present FPY distribution data along with existing bremsstrahlung-beam-induced photofission literature data [17, 19, 20, 26–30] for ^{238}U. The data marked with asterisks in the legends are the total mass-chain yield of fission products.
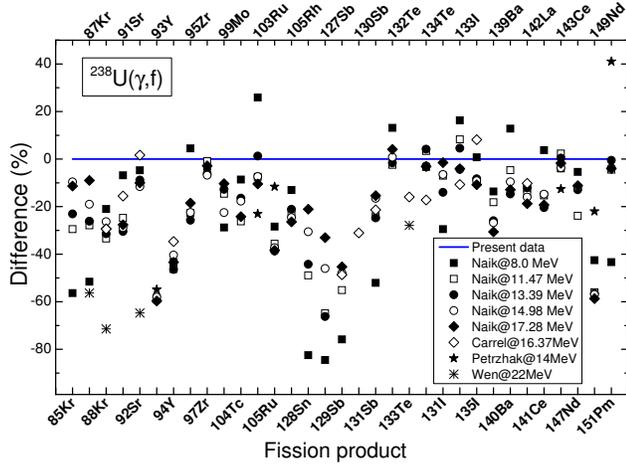

FIG. 14: (Color Online) Differences (in %) between the previous FPY values of several fission products in 8.0 - 22.0 MeV end-point bremsstrahlung-beam-induced fission of ^{238}U [19, 21, 27, 28, 30] and our present data are shown.

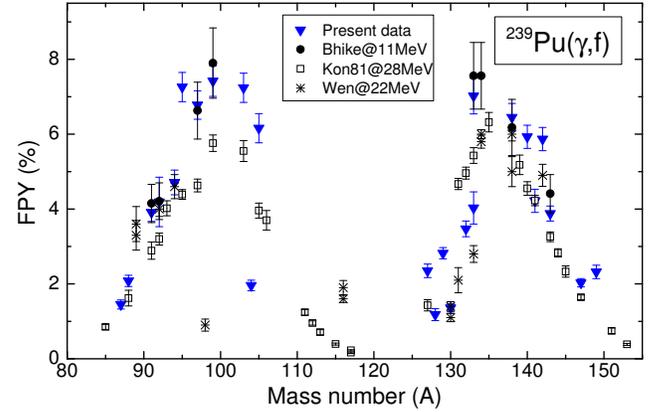

FIG. 15: (Color Online) FPY distributions of fission products in 22 [30] and 28-MeV [19] end-point bremsstrahlung-beam-induced fission of ^{239}Pu are compared with our present data obtained with monoenergetic photons at 13.0 MeV. Also shown in the plot are our previous [33] photofission data at 11.0 MeV. This measurement was based on a different experimental technique (see the text for detail).

imately 25% lower. It is interesting to note that the FPY data of Bhike *et al.* [33] agree fairly well with the present data. The data of Bhike *et al.* [33] are normalized to the ^{197}Au$(\gamma,n)^{196}$Au cross section.
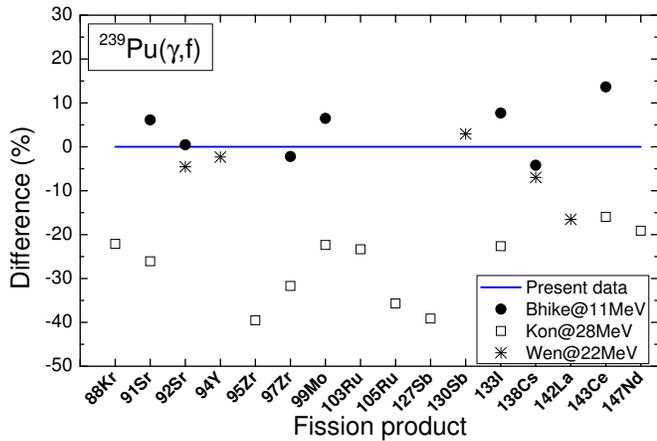
FIG. 16: (Color Online) Differences (in %) between the previous FPY values of several fission products in 11.0 and 22.0 MeV end-point bremsstrahlung-beam-induced fission of ^{239}Pu [30, 31] and our present data. Also shown in the figure are our previous data obtained in 11.0 MeV monoenergetic photofission.

V. COMPARISON TO NEUTRON-INDUCED FPY MEASUREMENTS

A. Same compound system

As pointed out in the introduction, the present work is part of a study to investigate the effect of the incoming probe (e.g., neutron versus photon) on nuclear fission observables [33, 35, 47, 48]. The present FPY values measured for the three systems, namely, ^{235}U$(\gamma,$f$)$, ^{238}U$(\gamma,$f$)$, and ^{239}Pu$(\gamma,$f$)$ are compared with previous measurements and/or evaluations for ^{234}U$(n,$f$)$, ^{237}U$(n,$f$)$, and ^{238}Pu$(n,$f$)$, respectively (Fig. 17) and are tabulated in Tables VI, VII, and VIII.

Unfortunately, data and evaluations are not available at the neutron energies of interest. In 1972 Nethaway and Mendoza [49] determined the FPY distributions from fission of ^{234}U with 14.8 MeV neutrons produced at the insulated-core-transformer accelerator at Lawrence Livermore Laboratory. The FPY values obtained in this work are systematically lower than our present FPY values except for a couple of fission products. Quantitatively, most of the present ^{235}U$(\gamma,$f$)$ FPY data are in reasonably good agreement with the average values obtained from the ENDF/B-VIII.0 evaluations at 0.5 and 14.0 MeV neutron energies. However, such a comparison can not be made for the other two reactions (^{237}U$(n,$f$)$ and ^{238}Pu$(n,$f$)$, for which evaluations only exist at 20 MeV neutron energy. Qualitatively, the comparison to these evaluations indicates good agreement. In 2000, Iyer et al. [50] measured the absolute yields of 27 fission products from the ^{238}Pu$(n,$f$)$ reaction with fast neutrons (average energy $\sim$ 1.9 MeV) from the highly enriched uranium-fueled swimming pool reactor APSARA. The

yield values of these products are systematically lower than our present values.

As indicated already, these comparisons (at different excitation energies) do not provide a solid conclusion, but give valuable information about the potential of $(\gamma,$f$)$ reactions to serve as a substitute for $(n,$f$)$ reactions on the appropriate target nuclei.

B. Same target system

Also, it is interesting to compare the FPYs obtained in neutron-induced fission to those in photon-induced fission on the same actinide nuclei, although the compound nuclei are not the same. Making a quantitative connection between the FPY distribution for fission of the same isotope induced with γ rays or neutrons at about the same excitation energy is relevant to applications requiring FPY data. This relationship could potentially allow the cumulative FPY data for $(n,$f$)$ measurements to be substituted in applications requiring $(\gamma,$f$)$ FPY values and vice versa.

Matching the excitation energies of the compound nuclei, the present 13.0 MeV ^{235}U$(\gamma,$f$)$ FPYs should be compared to ^{235}U$(n,$f$)$ FPYs at approximately $E_n = 6.5$ MeV. Neutron-induced FPY data on ^{235}U are available from the work of Gooden et al. [9, 51] at $E_n = 5.5$ MeV and their preliminary data at $E_n = 7.5$ MeV. They are shown in Fig. 18 (top panel) in comparison to our ^{235}U$(\gamma,$f$)$ FPYs. As can be seen more clearly in the bottom panel of Fig. 18, where the relative difference between the ^{235}U$(n,$f$)$ and ^{235}U$(\gamma,$f$)$ FPYs is shown, the average relative difference is approximately -15%. The FPY data are tabulated in Table IX.

A similar conclusion can be drawn from inspecting Fig. 19, which shows the comparison of ^{238}U$(n,$f$)$ and ^{238}U$(\gamma,$f$)$ FPYs. In this case, a neutron energy of $E_n = 8.2$ MeV will provide the same excitation energy of the compound nucleus ^{239}U as achieved with 13.0 photons in ^{238}U. FPY data at $E_n = 7.5$ MeV and 8.9 MeV are available from the work by Gooden et al. [9, 51] and Bhatia et al. [52], respectively. They are shown in Fig. 19 and tabulated in Table X.

Finally, Fig. 20 focuses on the comparison of the present ^{239}Pu$(\gamma,$f$)$ FPYs to those of the ^{239}Pu$(n,$f$)$ reaction. In this case $E_n = 6.5$ MeV matches the excitation energy of the ^{240}Pu and ^{239}Pu compound nuclei of interest. Therefore, as in Fig. 18, the present ^{239}Pu$(\gamma,$f$)$ data are compared in Fig. 20 to ^{239}Pu$(n,$f$)$ data at $E_n = 5.5$ MeV and $E_n = 7.5$ MeV. FPY values from the ^{239}Pu$(\gamma,$f$)$ and ^{239}Pu$(n,$f$)$ reactions are tabulated in Table XI. The approximately -15% difference observed in the bottom panels of Figs. 18, 19, and 20 is intriguing and deserves further study.

As discussed above, the present measured FPY values for the ^{235}U$(\gamma,$f$)$, ^{238}U$(\gamma,$f$)$, and ^{239}Pu$(\gamma,$f$)$ are in fairly good agreements with the corresponding values obtained for the ^{235}U$(n,$f$)$, ^{238}U$(n,$f$)$, and ^{239}Pu$(n,$f$)$ systems. We
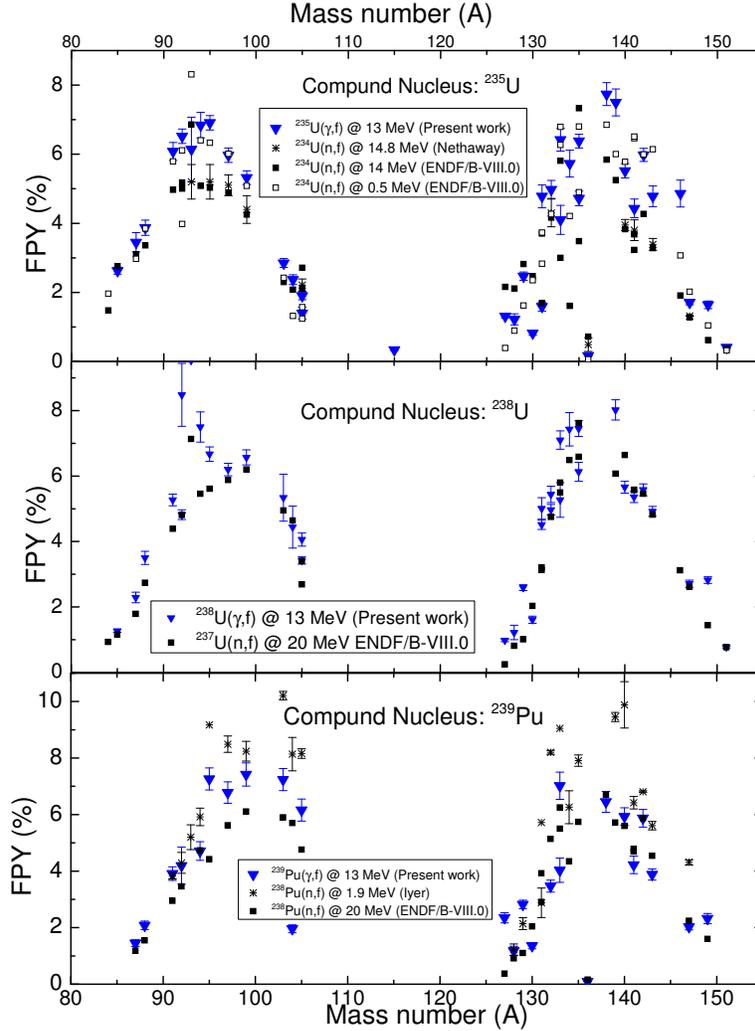
FIG. 17: (Color Online)Present FPY values obtained from ^{235}U(γ,f), ^{238}U(γ,f), and ^{239}Pu(γ,f) are compared with neutron-induced fission of ^{234}U, ^{237}U, and ^{238}Pu, respectively (providing the same compound nucleus in each case).

found that the average trend of the percent difference in the FPYs between fission induced with neutrons and γ-rays can be approximated with a linear function. The similarity of the (γ,f) and (n,f) FPY distributions is likely a consequence of the complexity of the nuclear decay paths that form the isotopes observed in the cumulative FPY distribution. That is, an isotope in the cumulative FPY distribution is normally fed from multiple branches that originate from different isotopes in the independent FPY distribution. In contrast to the independent FPYs, our results suggest that the cumulative FPYs are not very sensitive to the nuclear-structure details of the fissioning nucleus. This feature is likely due to the averaging effects of the decay chains that produce the cumulative FPYs.

VI. SUMMARY AND CONCLUSION

Fission product yields have been measured in photofission with a monoenergetic photon beam for the "big three" actinides ^{235}U, ^{238}U, and ^{239}Pu. The FPYs for these isotopes were obtained concurrently at $E_\gamma = 13.0$ MeV. Close to 40 fission products have been studied in the present work. The experimental approach, data-collection, and data-analysis procedures were very similar to those applied in our previous neutron-induced FPY measurements in the thermal to 15 MeV neutron energy range.

The present data are compared to FPYs determined with bremsstrahlung beams of different end-point energies ranging between approximately 8 MeV and 26 MeV. While for ^{235}U the FPYs obtained with bremsstrahlung beams agree fairly well with our data for the light products taken with monoenergetic photon beams, considerable scatter is observed in the data for the heavy products. Very large discrepancies are noticed for ^{238}U for almost all fission products investigated. The situation is similar for one of the two available ^{239}Pu data sets.

The comparison of the present FPYs obtained in photofission to those measured in neutron-induced fission of the "big three" actinides at the same excitation energy of the different compound nuclei reveals that the aver-

TABLE VI: FPY (in %) in 13 MeV monoenergetic photon-induced fission of ^{235}U along with their total uncertainties in comparison to measured and evaluated FPY values for the ^{234}U(n,f) system.

Product	FPY (%)				
	^{235}U(γ,f) Present work 13 MeV	^{234}U(n,f) Nethaway [49] 14.8 MeV	^{234}U(n,f) ENDF/B-VIII.0 [45] 0.5 MeV	14.0 MeV	JEFF-3.3 [45] 1.0 MeV
^{84}Br	1.77(13)	-	1.96	1.48	1.43
^{87}Kr	3.45(28)	-	2.96	3.10	3.38
^{88}Kr	3.87(22)	-	3.85	3.36	4.65
^{91}Sr	6.08(26)	-	5.79	4.97	6.04
^{92}Sr	6.52(21)	-	3.98	5.00	6.66
^{93}Y	6.14(93)	5.2(5)	8.31	6.86	8.82
^{94}Y	6.84(37)	-	6.40	5.08	7.53
^{95}Zr	6.91(21)	5.2(2)	6.33	5.03	7.05
^{97}Zr	5.97(21)	5.06(30)	6.01	4.89	6.50
^{99}Mo	5.32(20)	4.4(4)	5.08	4.25	5.74
^{104}Tc	2.37(14)	-	1.32	2.08	0.67
^{103}Ru	2.85(13)	-	2.42	2.30	1.36
^{105}Ru	1.90(11)	-	1.24	2.13	0.25
^{105}Rh	1.40(17)	2.21(18)	1.57	2.71	0.33
^{128}Sn	1.22(16)	-	0.89	2.11	0.57
^{127}Sb	1.31(5)	-	0.39	2.16	0.09
^{129}Sb	2.47(12)	-	1.62	2.82	0.82
^{130}Sb	0.82(6)	-	2.35	2.47	1.39
^{131}Sb	1.59(13)	-	2.83	1.69	1.97
^{132}Te	4.98(26)	4.3(4)	4.27	4.16	4.34
^{133}Te	4.10(42)	-	6.27	3.00	5.44
^{134}Te	5.37(39)	-	4.21	1.61	6.42
^{131}I	4.78(33)	-	3.73	3.70	2.59
^{133}I	6.42(33)	-	6.79	5.81	5.52
^{135}I	4.72(21)	-	4.90	3.48	6.44
^{135}Xe	6.38(20)	-	6.80	7.33	8.42
^{136}Cs	0.17(1)	0.49(2)	0.06	0.72	0.02
^{138}Cs^{g}	7.74(33)	-	6.85	5.84	8.08
^{139}Ba	7.50(39)	-	6.00	5.25	5.84
^{140}Ba	5.52(21)	3.95(16)	5.78	3.83	5.90
^{141}Ba	4.43(27)	-	6.46	3.32	5.62
^{142}La	5.98(19)	-	5.99	4.27	6.08
^{143}Ce	4.78(30)	3.39(17)	6.14	3.28	5.32
^{146}Pr	4.86(39)	-	3.07	1.91	2.76
^{147}Nd	1.71(7)	1.32(1)	2.02	1.28	2.28
^{149}Nd	1.64(11)	-	1.04	0.62	1.03
^{151}Pm	0.41(3)	-	0.32	0.36	0.35

age FPYs in photofission are approximately 15% larger than the average FPYs in neutron-induced fission. FPY data in photofission are needed at lower energies to find out whether the peculiar energy dependence discovered in neutron-induced fission for some fission products, especially ^{147}Nd [1], is also present in photofission.

Acknowledgments

TABLE VII: FPY (in %) in 13 MeV monoenergetic photon-induced fission of ^{238}U along with their total uncertainties in comparison to evaluated FPY values for the ^{237}U(n,f)^{238}U* system.

Product	FPY (%)	
	^{238}U(γ,f) Present work 13 MeV	^{237}U(n,f) ENDF/B-VIII.0 20.0 MeV
^{84}Br	2.49(19)	0.93
^{85}Kr^m	1.27(4)	1.16
^{87}Kr	2.29(16)	1.79
^{88}Kr	2.92(16)	2.74
^{91}Sr	5.27(18)	4.39
^{92}Sr	4.82(15)	4.81
^{92}Y	8.48(96)	4.81
^{93}Y	9.53(145)	7.13
^{94}Y	7.50(46)	5.46
^{95}Zr	6.67(22)	5.61
^{97}Zr	6.20(19)	5.88
^{99}Mo	6.57(22)	6.20
^{104}Tc	4.44(64)	4.64
^{103}Ru	5.34(72)	4.95
^{105}Ru	4.06(20)	2.69
^{105}Rh	3.42(11)	3.41
^{128}Sn	1.22(22)	0.81
^{127}Sb	0.98(4)	0.25
^{129}Sb	2.59(9)	1.01
^{130}Sb	1.61(11)	2.03
^{131}Sb	5.01(33)	3.13
^{132}Te	5.44(25)	4.75
^{133}Te	5.27(53)	5.80
^{134}Te	7.43(51)	6.49
^{131}I	4.51(14)	3.21
^{133}I	7.10(28)	5.50
^{135}I	6.13(29)	6.59
^{135}Xe	7.45(24)	7.62
^{139}Ba	8.02(31)	6.07
^{140}Ba	5.66(18)	6.64
^{142}La	5.58(18)	5.46
^{141}Ce	5.36(17)	5.58
^{143}Ce	4.92(15)	4.82
^{147}Nd	2.71(11)	2.62
^{149}Nd	2.82(10)	1.44
^{151}Pm	0.78(3)	0.77

[1] M.E. Gooden, C.W. Arnold, J.A. Becker, C. Bhatia, M. Bhike, E.M. Bond, T.A. Bredeweg, B. Fallin, M.M. Fowler, C.R. Howell, J.H. Kelley, Krishichayan, R. Marci, G. Rusev, C. Ryan, S.A. Sheets, M.A. Stoyer, A.P. Tonchev, W. Tornow, D.J. Vieira, and J.B. Wilhelmy, Nuclear Data Sheets **131**, 319 (2016).

[2] H. Goutte, J.F. Berger, P. Casoli, D. Gogny, Phys. Rev. C **71**, 024316 (2005).

[3] D.P. Wells, C.R. Segebade, P.L. Cole, AIP Conference Proceedings 1265, 379 (2010).

[4] J. Tickner, R. Bencardino, G. Roach, Nuclear Instruments and Methods in Physics Research Section B 268,

99 (2010).

[5] H. Naik, S.V. Suryanarayana, K.C. Jagadeesan, S.V. Thakare, P.V. Joshi, V.T. Nimje, K.C. Mittal, A. Goswami, V. Venugopal, S. Kailas, Journal of Radioanalytical and Nuclear Chemistry 295, 807 (2013).

[6] M. Gmar, F. Jeanneau, H. Makil, B. Poumaréde, F. Tola, Applied Radiation and Isotopes 63, 613 (2005).

[7] P.M. Dighe, E. Berthoumieux, D. Doré, J.M. Laborie, X. Ledoux, V. Macary, S. Panebianco, D. Ridikas, Annals of Nuclear Energy 36, 399 (2009).

[8] A.V. Varlamov, V.V. Varlamov, D.S. Ridenko, M.E. Stepanov, INDC(NDS)-394, 1999.

TABLE VIII: FPY (in %) in 13 MeV monoenergetic photon-induced fission of ^{239}Pu along with their total uncertainties. Also given are the evaluated FPY values for the ^{238}Pu(n,f)^{239}Pu* system.

Product	FPY (%)		
	^{239}Pu(γ,f)	^{238}Pu(n,f)	^{238}Pu(n,f)
	Present work	Iyer [50]	ENDF/B-VIII.0
	13 MeV	1.9 MeV	20.0 MeV
^{87}Kr	1.45(12)	-	1.18
^{88}Kr	2.08(15)	-	1.55
^{91}Sr	3.91(24)	3.82(1)	2.95
^{92}Sr	4.19(66)	4.29(37)	3.46
^{93}Y	-	5.20(44)	5.56
^{94}Y	4.71(33)	5.92(31)	4.73
^{95}Zr	7.26(39)	9.17	4.42
^{97}Zr	6.78(38)	8.49(29)	5.62
^{99}Mo	7.42(41)	8.24(35)	6.11
^{104}Tc	1.96(14)	8.14(59)	5.70
^{103}Ru	7.24(39)	10.21(15)	5.90
^{105}Ru	6.16(39)	8.16(17)	4.76
^{128}Sn	1.18(16)	1.22(20)	0.91
^{127}Sb	2.35(18)	-	0.37
^{129}Sb	2.82(15)	2.14(21)	1.10
^{130}Sb	1.36(11)	-	2.04
^{131}Sb	-	2.88(52)	2.91
^{132}Te	3.47(21)	8.20(7)	5.14
^{133}Te	4.03(43)	-	5.50
^{134}Te	-	6.26(58)	4.35
^{131}I	-	5.72	3.92
^{133}I	7.02(48)	9.05	6.25
^{135}I	-	7.91(20)	5.74
^{136}Cs	0.10(1)	-	0.16
^{138}Cs^g	6.45(37)	-	6.70
^{139}Ba	-	9.45(16)	5.72
^{140}Ba	5.93(31)	9.88(82)	5.60
^{141}Ba	4.22(31)	-	4.69
^{142}La	5.87(31)	6.81(3)	5.87
^{141}Ce	-	6.42(22)	4.79
^{143}Ce	3.88(20)	5.61(15)	4.54
^{147}Nd	2.03(11)	4.31(9)	2.24
^{149}Nd	2.32(18)	-	1.60

TABLE IX: FPY results obtained from photofission of ^{235}U at $E_\gamma = 13$ MeV and neutron-induced fission at $E_n = 5.5$ [9, 51] and 7.5-MeV [9, 51].

| Fission products	E_γ=13MeV Present data	E_n=7.5MeV Refs. [9, 51]	E_n=5.5MeV Refs. [9, 51]
^{91}Sr	6.08(26)	4.38(20)	-
^{92}Sr	6.52(21)	4.16(25)	-
^{95}Zr	6.91(21)	4.95(15)	5.92(30)
^{97}Zr	5.97(21)	5.02(14)	5.80(17)
^{99}Mo	5.32(20)	4.89(21)	5.67(27)
^{103}Ru	2.85(13)	2.54(9)	-
^{105}Ru	1.90(11)	1.82(6)	-
^{127}Sb	1.31(5)	0.85(5)	0.89(6)
^{132}Te	4.98(26)	4.01(24)	4.78(24)
^{131}I	4.78(33)	3.51(16)	4.14(19)
^{133}I	6.42(33)	5.20(22)	5.99(20)
^{135}Xe	6.38(20)	4.73(29)	-
^{140}Ba	5.52(21)	4.38(14)	4.87(16)
^{143}Ce	4.78(30)	3.89(20)	4.19(21)
^{147}Nd	1.71(7)	1.62(6)	1.92(10)
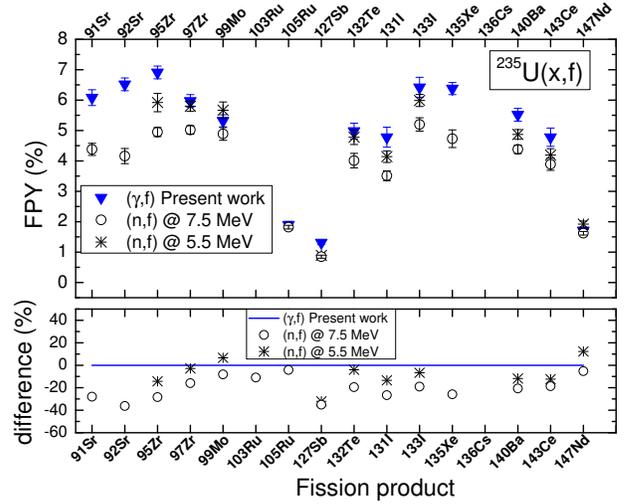
FIG. 18: (Color Online) FPY values obtained from photofission of ^{235}U are compared with neutron-induced fission of ^{235}U at 7.5, and 5.5-MeV [9, 51] in the top panel. The relative difference between the neutron-induced data and our data is shown in the bottom panel.

[9] M. Gooden, C. Arnold, M. Bhike, T. Bredeweg, M. Fowler, Krishichayan, A. Tonchev, W. Tornow, M. Stoyer, D. Vieira, and J. Wilhelmy, EPJ Web of Conference **146**, 04024 (2017).

[10] A. Tonchev, M. Stoyer, J. Becker, R. Macri, C. Ryan, S. Sheets, M. Gooden , C. Arnold, E. Bond, T. Bredeweg, M. Fowler, G. Rusev, D. Vieira, J. Wilhelmy, W. Tornow , C. Howell, C. Bhatia , M. Bhike, Krishichayan, J. Kelley, B. Fallin , S. Finch, The 6th International Conference on "Fission and Properties of Neutron-Rich Nuclei (ICFN6)", Sanibel Island, FL, Nov6, 2016.

[11] A.S. Soldatov and G.N. Smirenkin, Sov. J. Nucl. Phys. **55**, 1757 (1992); Report INDC(CCP) 359, 59 (1992).

[12] M.Ya. Kondrat'ko and K.A. Petrzhak, SJA **20**, 594 (1966) [English translation of Atomnaya Energiya **20**, 514 (1966).

[13] K.A. Petrzhak and G.A. Tyutin, Sov. J. Nucl. Phys. **9**, 556 (1969).

[14] D.C. Aumann and J.E. Gindler, J. Inorg. Nucl. Chem. **32**, 731 (1970).

[15] M.Ya. Kondrat'ko, V.N. Korinets, and K.A. Petrzhak, Journal of SJA **35** 866 (1973) [English translation of Atomnaya Energiya **35** 214 (1973).

[16] K.A. Petrzhak, E.V. Platygina, Yu.A. Solov'ev, and V.F. Teplykh, Journal of SJA **41**, 654 (1976) [[English translation of Atomnaya Energiya **41**, 44 (1976).

[17] H. Thierens, D. De Frenne, E. Jacobs, A. De Clercq, and A.J. Deruytter Phys. Rev. C **14**, 1058 (1976).

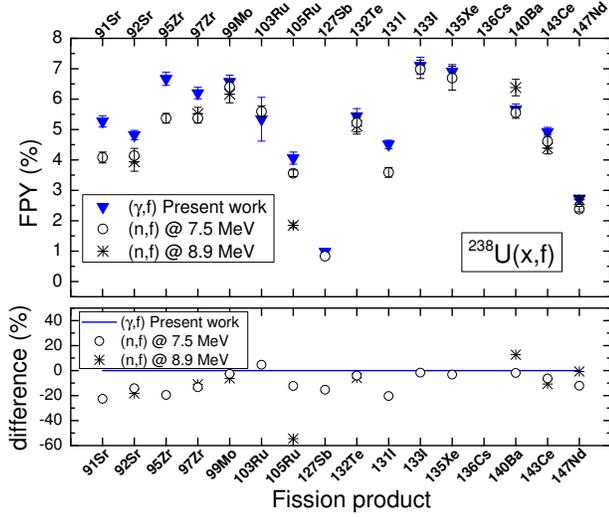[18] E. Jacobs, H. Thierens, D. De Frenne, A. De Clercq, P.D'hondt, P. de Gelder, and A.J. Deruytter, Phys. Rev.

FIG. 19: (Color Online)FPY values obtained from photofission of ^{238}U are compared with the neutron-induced fission of ^{238}U at 8.9 and 7.5-MeV [9, 51, 52] in the top panel. The relative difference of the neutron-induced data and our data is shown in the bottom panel.

FIG. 20: (Color Online) FPY values obtained from photofission of ^{239}Pu are compared with neutron-induced fission of ^{239}Pu at 7.5 and 5.5-MeV [9, 51] in the top panel. The relative difference of the neutron-induced data and our data is shown in the bottom panel.

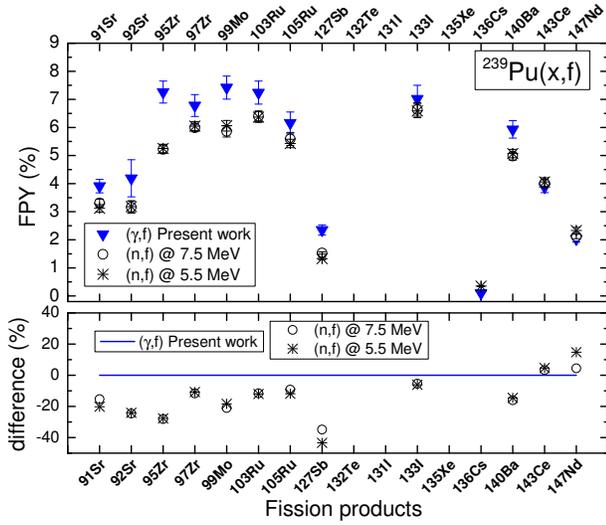TABLE X: FPY results obtained from photofission of ^{238}U at $E_\gamma = 13$ MeV and neutron-induced fission at 7.5 [9, 51] and 8.9 MeV [52].

Fission products	E_γ=13MeV Present data	E_n=8.9MeV Ref. [52]	E_n=7.5MeV Refs. [9, 51]
^{91}Sr	5.27(18)	-	4.08(18)
^{92}Sr	4.82(15)	3.94(31)	4.14(24)
^{95}Zr	6.67(22)	-	5.37(16)
^{97}Zr	6.20(19)	5.52(21)	5.37(16)
^{99}Mo	6.57(22)	6.16(28)	6.40(24)
^{103}Ru	5.34(72)	-	5.59(19)
^{105}Ru	4.06(20)	1.85(8)	3.56(11)
^{127}Sb	0.98(4)	-	0.83(5)
^{132}Te	5.44(25)	5.12(27)	5.22(30)
^{131}I	4.51(14)	-	3.59(16)
^{133}I	7.10(28)	-	6.98(30)
^{135}Xe	6.91(23)	-	6.69(39)
^{140}Ba	5.66(18)	6.38(27)	5.55(18)
^{143}Ce	4.92(15)	4.39(19)	4.61(23)
^{147}Nd	2.71(11)	2.69(15)	2.38(9)

TABLE XI: FPY results obtained from photofission of ^{239}Pu at $E_\gamma = 13$ MeV and neutron-induced fission at $E_n = 5.5$- [9, 51], and 7.5- [9, 51]

Fission products	E_γ=13MeV Present data	E_n=7.5MeV Refs. [9, 51]	E_n=5.5MeV Refs. [9, 51]
^{91}Sr	3.91(24)	3.31(14)	3.12(13)
^{92}Sr	4.19(66)	3.16(21)	3.18(21)
^{95}Zr	7.26(39)	5.22(15)	5.25(15)
^{97}Zr	6.78(38)	5.99(14)	6.05(16)
^{99}Mo	7.42(41)	5.86(20)	6.06(19)
^{103}Ru	7.24(39)	6.40(19)	6.37(19)
^{105}Ru	6.16(39)	5.59(23)	5.43(15)
^{127}Sb	2.35(18)	1.53(4)	1.33(4)
^{133}I	7.02(48)	6.64(24)	6.59(24)
^{136}Cs	0.10(1)	-	0.35(2)
^{140}Ba	5.93(31)	4.98(14)	5.07(15)
^{143}Ce	3.88(20)	4.01(14)	4.06(15)
^{147}Nd	2.03(11)	2.12(8)	2.33(11)

translation of Yardernaya Fizika **14**, 950 (1970)].

[22] A. Alm and T. Kivikas, Nucl. Phys. **A215**, 461 (1973).

[23] E. Jacobs, H. Thierens, D. De Frenne, A. De Clercq, P.D'hondt, P. de Gelder, and A.J. Deruytter, Phys. Rev. C **19**, 422 (1979).

[24] S. Kahane and A. Wolf, Phys. Rev. C **32**, 1944 (1985).

[25] Yu.P. Gangrsky, V.I. Zhemenik, N.Yu. Maslova, G.V. Mishinsky, Yu.E. Penionzhkevich, O. Szollos J. PAN **66**, 1211 (2003) [English translation of Yadernaya Fizika **66**,1251 (2003).

[26] H.Naik, V.T. Nimje, D. Raj, S.V. Suryanarayana, A. Goswami, S. Singh, S.N. Acharya, K.C. Mittal, S. Ganesan, P.Chandrachoodan, V.K.Manchanda, V.Venugopal, and S. Banarjee, Nucl. Phys. A **853**, 1 (2011).

[27] H. Naik, F. Carrel, G.N. Kim, F. Laine, A. Sari, S. Normand, A. Goswami, Eur. Phys. J. A **49**, 94 (2013).

[28] H. Naik, B.S. Shivashankar, H.G. Raj Prakash, Deves

C **21**, 237 (1980).

[19] F. Carrel, M. Agelou, M. Gmar, F. Laine, J. Loridon, J.-L. Ma, C. Passard, and B. Poumarede, IEEE Transactions on Nucl. Sci. **58**, 2064 (2011).

[20] K.A. Petrzhak and P.V. Sedletskiy, Soviet Journal of Nuclear Physics **15**, 1025 (1963) [English translation of J. Atomnaya Energiya **15**, 308 (1963)].

[21] K.A. Petrzhak, V.F. Teplykh, M.G. Pan'yan, and V.A. Demin, Soviet J. of Nucl. Phys. **14**, 532 (1971) [English

Raj, G. Sanjeev, N. Karunakara, H.M. Somashekarappa, S.Ganesan, G.N.Kim, and A.Goswami, J. Radioanal. Nucl. Chem. **299**, 127 (2014).

[29] S.S. Belyshev, B.S. Ishkhanov, A.A. Kuznetsov, and K.A. Stopani, Phys. Rev. C **91**, 034603 (2015).

[30] X. Wen and H. Yang, Nucl. Instrum. Methods Phys. Res. Sec. A **821**, 34 (2016).

[31] M.Ya. Kondrat'ko, V.N. Korinets, and K.A. Petrzhak, SJA **40**,83 (1976).

[32] M.Ya. Kondrat'ko, A.V. Mosesov, K.A. Petrzhak, and O.A. Teodorovich, SJA **50**, 41 (1981) [English of AE50,34 (1981).

[33] M. Bhike, W. Tornow, Krishichayan, A.P. Tonchev, Phys. Rev. C **95**, 024608 (2017).

[34] N. Bohr and J.A. Wheeler, Phys. Rev. **56**, 426 (1939).

[35] Krishichayan, M. Bhike, A.P. Tonchev, and W. Tornow EPJ Web of Conference **146**, 04018 (2017).

[36] H.R. Weller, M.H. Ahmed, H. Gao, W. Tornow, Y.K. Wu, M. Gai, and R. Miskimen, Progress in Particle and Nuclear Physics **62**, 257 (2009).

[37] Krishichayan, M. Bhike, W. Tornow, A.P. Tonchev, and T. Kawano, Phys. Rev. C **96**, 044623 (2017).

[38] I. Newsome, M. Bhike, Krishichayan, and W. Tornow, Phys. Rev. C **97**, 044617 (2018).

[39] A.P. Tonchev, C.T. Angell, M. Boswell, A.S. Crowell, B. Fallin, S. Hammond, C.R. Howell, A. Hutcheson, H.J. Karwowski, J.H. Kelley, R.S. Pedroni, W. Tornow, J.A. Becker, D. Dashdorj, J. Kenneally, R.A. Macri, M.A. Stoyer, C.Y. Wu, E. Bond, M.B. Chadwick, J. Fitzpatrick, T. Kawano, R.S. Rundberg, A. Slemmons, D.J. Vieira, and J.B. Wilhelmy, Phys. Rev. C **77**, 054610 (2008).

[40] C. Bhatia, B. Fallin, M.E. Gooden, C.R. Howell, J.H. Kelley, W. Tornow, C.W. Arnold, E.M. Bond, T.A. Bre-

deweg, M.M. Fowler, W.A. Moody, R.S. Rundberg, G. Rusev, D.J. Vieira, J.B. Wilhelmy, J.A. Becker, R. Macri, C. Ryan, S.A. Sheets, M.A. Stoyer, and A.P. Tonchev, Nuclear Instruments and Methods in Physics Research Section A **757**, 7 (2013).

[41] J.A. Grundl, D.M. Gilliam, N.D. Dudey, and R.J. Popek, Nuclear Technology **25**, 237 (1975).

[42] www.canberra.com

[43] J.T. Caldwell, E.J. Dowby, B.L. Berman, R.A. Alvarez, and P. Meyer, Phys. Rev. C **21**, 1215 (1980).

[44] Eckert & Ziegler, www.ezag.com/home/products/isotope-products.html

[45] http://www.nndc.bnl.gov/

[46] D.C. Radware, Nuclear Instruments and Methods in Physics Research Section A **361**, 297 (1995) and www.radware.phy.ornl.gov

[47] Krishichayan, M. Bhike, S.W. Finch, C.R. Howell, A.P. Tonchev, and W. Tornow, Nucl. Instrum. Methods Phys. Res. Sec. A **854**, 40 (2017).

[48] Krishichayan, S.W. Finch, C.R. Howell, A.P. Tonchev, and W. Tornow, Phys. Rev. C **98**, 014608 (2018).

[49] D.R. Nethaway and b. Mendoza, Phys. Rev. C **6**, 1821 (1972).

[50] R.H. Iyer, H. Naik, A.K. Pandey, P.C. Kalsi, R.J. Singh, A. Ramaswami, and A.G.C. Nair, Nuclear Science and Engineering **135**, 227 (2000).

[51] M. Gooden, private communication

[52] C. Bhatia, B.F. Fallin, M.E. Gooden, C.R. Howell, J.H. Kelley, W. Tornow, C.W. Arnold, E. Bond, T.A. Bredeweg, M.M. Fowler, W. Moody, R.S. Rundberg, G.Y. Rusev, D.J. Vieira, J.B. Wilhelmy, J.A. Becker, R. Macri, C. Ryan, S.A. Sheets, M.A. Stoyer, and A.P. Tonchev, Phys. Rev. C **91**, 064604(2015).